Environ Sci Pollut Res (2016) 23:7278–7287
DOI 10.1007/s11356-015-5945-x

RESEARCH ARTICLE

Semi-continuous sampling of health relevant atmospheric particle subfractions for chemical speciation using a rotating drum impactor in series with sequential filter sampler

Fengxia Li[1,2] · Jürgen Schnelle-Kreis[1] · Erwin Karg[1] · Josef Cyrys[3,4] · Jianwei Gu[4] · Jürgen Orasche[1,2] · Gülcin Abbaszade[1] · Annette Peters[3,5] · Ralf Zimmermann[1,2]

Received: 24 August 2015 / Accepted: 7 December 2015 / Published online: 17 December 2015

Abstract To achieve unattended continuous long-term (eg., 1 week) sampling of size-segregated 24-h ambient particulate matter (PM), a sampling strategy of a modified 3-stage rotating drum impactor (RDI) in series with a sequential filter sampler was introduced and verified in a field campaign. Before the field sampling, lab experiment was conducted to test the collection efficiency of the third stage of the RDI using the quartz-fiber filter (QFF) as the substrate. The measured value is 0.36 μm, which is larger than the nominal value 0.1 μm. A fast direct analysis of organic species in all size fractions (<0.36, 0.36–1, 1–2.4, and 2.4–10 μm) of 24-h ambient samples was done using in situ derivatization thermal desorption gas chromatography time-of-flight mass spectrometry (IDTD-GC-TOFMS). A few secondary originated polar markers (dicarboxylic acids, cis-pinonic acid, etc.) were introduced and evaluated using this method for the first time and quantified simultaneously with polycyclic aromatic hydrocarbons (PAH) in the filter samples (<0.36 μm). For the other RDI strip samples (0.36–1, 1–2.4, and 2.4–10 μm), PAH and levoglucosan were quantified. The comparability of two such sampler sets was verified with respect to the PM collection profile of the two RDIs as well as measured concentration of chemical compounds in each sampled size fraction, so that a future epidemiological study on the relationship between the finest PM/its chemical composition and health outcome could be carried out through parallel sampling at two sites. The internal correlations between the size-segregated organic compounds are discussed. Besides, the correlations between the size-segregated organic species and size-segregated particulate number concentration (PNC) as well as meteorological parameter are discussed as well.

Keywords Size-segregated particulate matter · PAH · Polar markers · Rotating drum impactor · Chemical speciation · In situ derivatization thermal desorption

Responsible editor: Gerhard Lammel

Electronic supplementary material The online version of this article (doi:10.1007/s11356-015-5945-x) contains supplementary material, which is available to authorized users.

✉ Jürgen Schnelle-Kreis
juergen.schnelle@helmholtz-muenchen.de

Fengxia Li
fengxia.li@helmholtz-muenchen.de

[1] Joint Mass Spectrometry Center, Cooperation Group Comprehensive Molecular Analytics, Helmholtz Zentrum München, Neuherberg, Germany

[2] Joint Mass Spectrometry Center, Chair of Analytical Chemistry, University of Rostock, Rostock, Germany

[3] Institute of Epidemiology II, Helmholtz Zentrum München, German Research Center for Environmental Health, Neuherberg, Germany

[4] Environmental Science Center (WZU), University of Augsburg, Augsburg, Germany

[5] Department of Environmental Health, Harvard T.H. Chan School of Public Health, Boston, MA, USA

Introduction

The ambient particulate matter (PM) sampling techniques in many cases collect PM smaller than 10 μm (PM_{10}), 2.5 μm ($PM_{2.5}$), or sometimes 1 μm (PM_1) on filter substrates. Due to the rising concern of adverse health effect of PM within accumulation mode (<500 nm) and ultrafine (<100 nm) size range (Kelly and Fussell 2012), further differentiation of PM in the size range below 2.5 μm is necessary. For this purpose, cascade impactors which have a long history for particulate matter sampling are frequently used (Marple 2004; Marple and

Willeke 1976). To study the link between the ultrafine particle composition and adverse health effects, the separate sampling of the accumulation mode and ultrafine PM is desired as it predominantly holds the freshly emitted particle fraction from anthropogenic combustion sources (Gu et al. 2011). Thus, separating the accumulation mode and ultrafine PM may offer a better data base for correlation of PM properties with health outcomes.

The rotating drum impactor (RDI) is a special category of slit cascade impactors originally designed by Lundgren (Lundgren 1967) for time- and size-resolved sampling of PM. In contrast to the conventional flat impaction plate, a rotating drum is used as the substrate holder. It automatically rotates a specific step after a certain time interval set by the user and collects samples on a new substrate position. Using a series of such drum impaction stages, an RDI can provide size- and time-resolved PM samples simultaneously. Usually, impactors are designed to separate ambient PM into very small size fractions, such as microorifice uniform deposit impactor (MOUDI) or electrical low-pressure impactor (ELPI). However, an elaborate fractionation may result in prolonged sampling times with all its negative effects on the chemical conditions of the individual samples or in a reduced quantity of sample mass which may be close to or even below the detection limit of the chemical analysis method (Sanderson et al. 2014). Additionally, the samples on the lower stages are often exposed to low pressure to achieve the high impaction velocity. This, however, alters the sample conditions, especially with respect to the disintegration and potential evaporation of semi-volatile components (Kavouras and Koutrakis 2001). Thus, the reduced PM size resolution capability of a 3-stage RDI together with a tolerable pressure drop at the last stage may be a benefit for ambient PM sampling with subsequent chemical component analysis. Additionally, for practical purposes during field campaigns and long-term ambient PM sampling, wider nozzles and repetitive position changes on the substrate reduce the risk of blocking the nozzle and enhance sampling stability and data comparability.

By default, the RDI can be equipped with a single backup filter to collect the finest particles while it automatically moves the drums and continues sampling without stopping or interrupting the sample flow. In our application, the backup filter after the last drum was removed and the RDI was connected to a sequential filter sampler in series to achieve an automatic change of the backup filter. Thereby, the drums and backup filters can be synchronized to start sampling and switch to new samples simultaneously.

It has been observed in other studies that the particle collection characteristics of impactors are altered when a thick porous material is used as a substrate instead of a dense film or foil. Normally, the porous substrate will shift the cutoff diameter towards smaller diameters and also reduce the sharpness of the cutoff curve (Demokritou et al. 2004; Kavouras and Koutrakis 2001; Lee et al. 2005; Rao and Whitby 1978; Saarikoski et al. 2008; Sillanpaa et al. 2004). However, sometimes, the usage of porous substrates such as quartz-fiber filter (QFF) or polyurethane foam (PUF) is preferable to mitigate problems like overload, particle bounce off, and re-entrainment (Demokritou et al. 2004; Lee et al. 2005; Rao and Whitby 1978). For the intended 24-h ambient PM sampling, especially the overload was a major concern. Additionally, from the analytical point of view, an identically prepared substrate like QFF for both impactor and filter samples is preferable and it also avoids the usage of adhesive coatings, which interfere with chemical analysis (Wang et al. 2014).

To meet the requirements of the future epidemiological studies, data from at least two different sites (reference and roaming) in parallel are required. Therefore, the first objective of the present study was to prove that sampling with two sets of such combinations of commercially available RDIs and sequential samplers deliver comparable results in terms of chemical composition of the collected size-segregated samples.

Organic chemical compound analysis of size-segregated ambient PM is challenging. First, the size-fractioned sampling generates an elevated number of samples, thereby requiring an analytical method of high throughput to deal with the analytical workload. Second, the total PM mass is divided into several fractions thereby reducing the compound amounts in each fraction and challenge for analytical sensitivity in the case of trace chemical marker compound analysis. Prolonging the sampling time to several days or combining several samples were common ways in order to analyze the size distribution of organic compounds such as polycyclic aromatic hydrocarbons (PAH) (Di Filippo et al. 2010; Park et al. 2007; Rogula-Kozlowska 2014; Saarnio et al. 2008; Sahu et al. 2008). Solvent extraction-based methods are widely used to analyze the size-fractionated PM target compounds. Direct sample analysis can be a good solution to overcome these two difficulties. Firstly, it saves sample preparation time, and secondly, more sample portions can be introduced for a single analysis. Therefore, another objective of this study is to apply the in situ derivatization thermal desorption gas chromatography time-of-flight mass spectrometry (IDTD-GC-TOF-MS) (Orasche et al. 2011) method used for a routine chemical marker analysis of ambient particle samples by our group to size-segregated samples. Additionally for this objective, the analysis of a couple of polar compounds mostly associated with the secondary organic aerosol was introduced and integrated in this method.

Methods

Collection characteristics of the RDIs

The 3-stage RDIs used in our study were manufactured by the Swiss Federal Laboratories for Materials Science and Technology (Empa, Dübendorf, Switzerland) and have been used in previous studies for time and size-segregated PM sampling and analysis (Bukowiecki et al. 2007; Bukowiecki et al. 2005; Richard et al. 2010; Richard et al. 2011). The nominal midpoint cutoff diameters at three stages are given to be 2.5, 1, and 0.1 μm, respectively. Bukowiecki et al. verified the deposition uniformity by this impactor. They also tested the 50 % aerodynamic cutoff diameters to be 2.4 and 1.0 μm for the first and second stages, respectively (Bukowiecki et al. 2009). In the following text, these two values are used as the midpoint cutoff diameters of stage 1 and 2, respectively.

Focusing on the PM in the accumulation mode and ultrafine size range, i. e., the PM on the backup filter behind the third stage, the cutoff behavior of the third stage is critical for the comparability and future data interpretation in our studies. Additionally, the collection characteristics with QFF as the substrate should be verified. Therefore, the size-dependent collection efficiencies of both RDIs used in the study were tested using indoor particles.

In an experimental setup (Fig. 1a), indoor aerosol was pumped through the RDI at the nominal flow rate of 16.7 l min^{-1}. A differential mobility analyzer (DMA; model 3081, TSI Inc., Shoreview, USA) and condensation particle counter (CPC; model 3025A, TSI Inc., Shoreview, USA) were connected to the outlet of the RDI to determine the PM size distribution. The DMA and CPC were calibrated with latex standard spheres (Distrilab, Leusden, The Netherlands) prior to measurement. Size distribution with the impactor was determined with an ungreased aluminum foil or QFF-covered drum installed at the last stage, reference distributions with empty drum housings, i. e., with all the drums removed. The collection efficiency (C_{Dp}) was calculated for each size channel of the DMA using Eq. (1).

$$C_{Dp} = 1 - \frac{C_{N,\text{ with last drum}}}{C_{N,\text{ no drum}}} \quad (1)$$

As the underpressure behind the third nozzle was only about −100 hPa, the CPC counting data was used without correction due to the following considerations: (i) both number distributions (with and without drum) were measured at the same pressure level, as the nozzle makes the pressure drop independently of the presence of the drum and the nozzle was installed in both cases; (ii) according to Hermann and Wiedensohler, the CPC counting efficiency is nearly unaffected by the underpressure down to 400 hPa (Hermann and Wiedensohler 2001) for particles >30 nm; and (iii) Seifert et al. tested the sizing of an scanning mobility particle sizer (SMPS) between 1000 and 400 hPa ambient pressure, showing only minor deviations for the 900 hPa pressure level (Seifert et al. 2004).

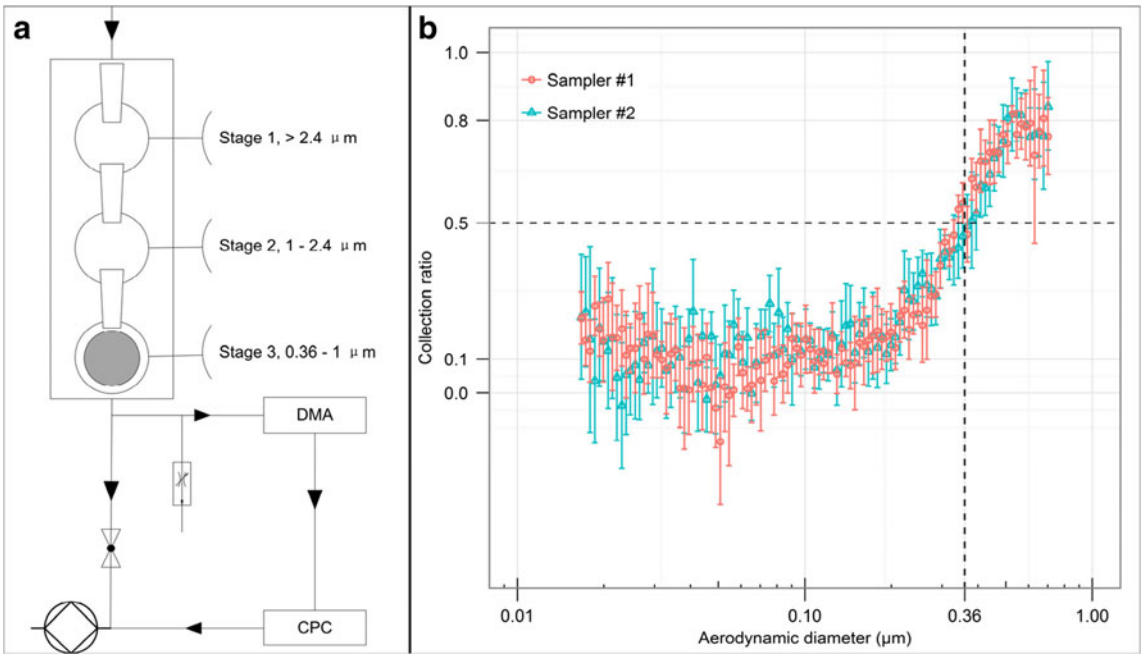

Fig. 1 **a** Experimental set up to test the collection efficiency of the RDIs' last impaction stage. **b** Collection efficiency curves of both RDIs' last impaction stage using QFF as impaction substrate

Parallel field sampling

The field sampling was performed in parallel, to test the comparability of sampling as well as analysis methods. The field sampling setup is shown in Fig. 2a. Each RDI was adapted as a pre-impactor to the subsequent filter sampler (Partisol™ 2025i Sequential Air Sampler, Thermo Scientific, USA). The RDI was mounted vertically on top of the filter sampler. The airflow after the third stage of the RDI was directed straight down to the filter without any bending. The sampling flow rate was controlled by the filter sampler to be 16.7 l min^{-1} which is also the nominal flow rate of the RDI. Both combination sets were placed side by side for multiple 24-h sampling periods at the ambient aerosol monitoring station in the campus of the University of Applied Sciences Augsburg (Augsburg, Germany). A detailed description of the sampling site and surroundings can be found in previous publications (Pitz et al. 2008a; Pitz et al. 2008b).

Each drum of the RDIs was tightly covered with QFF strips being identical to the filter with respect to the matrix composition and structure. Both drum strips and backup QFF filters (T293, Munktell, Grycksbo, Sweden) were baked at 500 °C overnight before usage. Once started, the filter sampler will load new filter and the drums will switch to new position for a new sample simultaneously and automatically at the interval of 24 h. It is worth mention that this interval could also be changed and synchronized from both filter sampler and RDI to adjust to other applications. Filters and drum samples were collected from the samplers once a week. Samples were taken between 25th March and 10th April, 2014 (Online Resource 1 Table S1). In total, 12 days of valid parallel sample pairs were available for chemical analysis (Table S1).

Meteorological data monitoring

The meteorological parameters including air temperature, relative humidity, wind speed, and wind direction were measured by the Bavarian Environmental Agency (Bayerisches Landesamt für Umwelt, LfU). The LfU site is located 4 km south to the city center.

Particle number concentration measurement

Particle size distribution (PSD) from 5 nm to 10 μm was determined by a combination of a customized twin differential mobility particle sizer (TDMPS) and an aerodynamic particle sizer (APS) (Pitz et al. 2008a). The size-segregated particulate number concentration (PNC) was calculated for the size ranges of 5–50, 50–360, 360–1000 nm, 1.0–2.4 and 2.4–10 μm, respectively.

Organic species measurement

The chemical components of PM collected on drum strips as well as the filters were analyzed by IDTD-GC-TOF-MS method (Orasche et al. 2011). A brief description of the method can be found in the Online Resource 1.

The method was proven to be able to quantify polycyclic aromatic hydrocarbons (PAH), oxygenated PAH, alkylated PAH, and some acids and polyols generated by wood combustion such as abietic acid and levoglucosan (Orasche et al. 2011). For the present study, a few secondary originated polar compounds were evaluated additionally and integrated into the compounds' calibration procedure for the first time to our knowledge, including dicarboxylic acids, cis-pinonic acid, 3-hydroxyglutaric acid, 3-methyl-1,2,3-butanetricarboxylic acid (3-MBTCA), 2-methylerytheritol, 4-nitrophenol, and 4-nitrocatechol. Authentic 3-MBTCA was used for

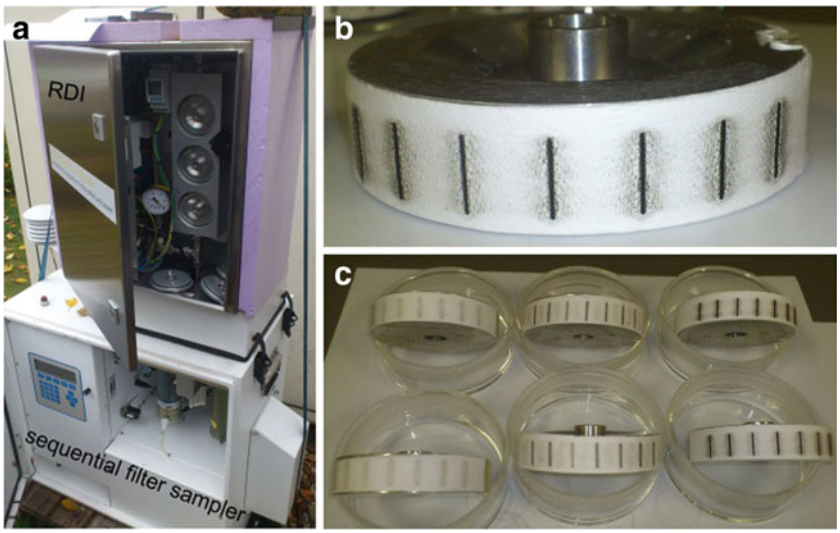

Fig. 2 **a** One of the two sets of samplers were operated in parallel during the sampling period at the reference site in University of Applied Sciences Augsburg. **b** Stage 3 loaded with seven daily ambient PM samples. **c** All three stages of both RDIs loaded with samples

identification only. Quantification of 3-MBTCA was based on the calibration curve of 3-hydroxyglutaric acid, which has a similar structure.

Results and discussion

Comparison of both samplers

Collection characteristics of the RDIs' last stages

The collection efficiency curves of the third stage for both RDIs are shown in Fig. 1b. In this figure, the measured electrical mobility diameter by the SMPS is calculated to aerodynamic diameter using an estimated aerosol density ρ_p = 1.4 g cm^{-3} based on our measurement condition (Pitz et al. 2003; Pitz et al. 2008b). The means and the standard deviations (10 repetitions from RDI #2, 5 repetitions from RDI #1) are shown in Fig. 1b. The graphs show that both RDIs have very similar collection patterns.

The midpoint collection diameter ($C_{Dp,\ 50\%}$) is calculated by fitting each collection curve with a sigmoid function curve. *T* test was applied to 10 calculated $C_{Dp,\ 50\%}$ values from RDI #1 and 5 values from RDI #2. The *t* value is 0.408 and *p* value is 0.69; no significant difference could be demonstrated between the midpoint collection diameters of both RDIs at a significance level of 0.05. Besides, from the graph, we could not find any systematical shift between the two collection curves either. To mention that, there was a time delay between the measurements of the two aerosol distributions used to calculate the collection curve, which makes the calculation sensitive to the indoor PM distribution change. The average $C_{Dp,\ 50\%}$ of the third stage was found to be about 0.36 μm aerodynamic diameter using 1.4 g cm^{-3} to represent the density of the measured aerosol. The average electrical mobility $C_{Dp,\ 50\%}$ diameter is around 0.30 μm from the SMPS measurement. Therefore, the real $C_{Dp,\ 50\%}$ of the RDI might be slightly different from 0.36 μm due to the deviation of the real density from our estimation. This small uncertainty of the midpoint collection diameter due to the uncertain of the real density value shall not make a big influence on the interpretation of chemical speciation data. For following data interpretation and comparison, 0.36 μm is used as the midpoint collection diameter. This value is much larger than the nominal cutoff diameter of 0.1 μm. Calculated stokes number is 0.366. The summary of the four size fractions sampled then would be <0.36, 0.36–1, 1–2.4, and 2.4–10 μm.

Influence on the collection efficiency when using the QFF substrate

It can be observed from Fig. 1b that at around 600 nm, the collection efficiency reaches its maximum of about 80 %. It has been repeatedly reported in other studies that porous material facilitates the collection efficiency by decreasing the midpoint cutoff diameter as well as mitigating the bouncing off and re-entrainment artifact. From our test using aluminum foil as a substrate, an increased $C_{Dp,\ 50\%}$ value in the collection curve as well as lower maximum collection efficiency are observed (see Online Resource 1 Fig. S1). This reveals the low collection capacity of the ungreased aluminum substrate as well as high sampling artifact, at least during the sampling start period without a substantial loading of ambient particles on the substrate. As mentioned, greasing of the aluminum foils is problematic for our study because of the interference with organic compound speciation. Figure 1b also shows that, around 10 % of the particles <200 nm is additionally collected. The excess collection characteristic of QFF substrate is probably due to the other effects instead of impaction, for instance, the penetration of the aerosols into the fiber layer at high velocity (Kavouras and Koutrakis 2001; Rao and Whitby 1978) or the diffusion losses to the surface of the filter material. During the further traveling process of the PM, some particles may be trapped by filtration mechanisms such as interception or diffusion (Sillanpaa et al. 2004). As is shown in Fig. 1b that for particles <50 nm, the collection ration increases with decreasing of particle size, this is an indication that the main collection mechanism for these smallest particles is diffusion. In the view of the field campaign sampled strips in Fig. 2b, specifically, there was a residue of PM spreads out on both sides of the central impacted strips. This "shadow" may cause slight underrepresentation of the <0.36 μm PM collected on the filter.

Organic species analysis results

Quantified organic species

Organic composition including PAH and levoglucosan were investigated from the filters as well as the three RDI stages. For coarse particles (2.4–10 μm), only the comparatively volatile pyrene, fluoranthene, and levoglucosan were detected, the other PAH with higher molecular weight were below the limit of quantification (LOQ) (see measured compounds and their LOQ values in Online Resource 1 Table S2). Therefore, this fraction was not included in the following discussion. Polar markers except levoglucosan were only quantified in the smallest fraction samples (<0.36 μm) as derivatization for these markers from the RDI samples was not reproducible. 2-methylerytheritol, a tracer of isoprene photooxidation (Claeys et al. 2004), was not included in the discussion because it was not detected for most of the samples.

Comparability of samples from both samplers sets

A paired *t* test of daily value from both sampling sets was applied to statistically evaluate the comparability on each individual compound level. The result is shown in Online Resource 1 Tables S3 and S4. No evidence of significant differences could be found for nearly all the measured compounds in all size fractions ($\alpha = 0.05$). The only exception is that fluoranthene and pyrene concentrations in the size fraction <0.36 μm from sampler #1 are significantly lower than from those in sampler #2. Of all the quantified PAH, these two have the highest volatility, what might have led to a loss during sample transport, storage, or preparation.

Figure 3 shows that measured pairs of samples coincide with the 1:1 line very well with a limited random variation in both directions. Polar markers are found at higher concentration than PAH; while levoglucosan originating mainly from wood combustion shows the highest concentration. Besides, polar compounds somehow diverge more from the 1:1 line, which most probably results from a lower analytical reproducibility of the derivatization. With regard to these compounds, full derivatization of multiple functional groups is necessary to have good quantification results. The comparable results discussed above give a strong indication that there is no systematic different behavior between the two sampling sets. This warranted the plan to investigate spatial variability of chemical species in ultrafine and lower accumulation mode PM and their relation with health outcome by collecting parallel samples at different sites.

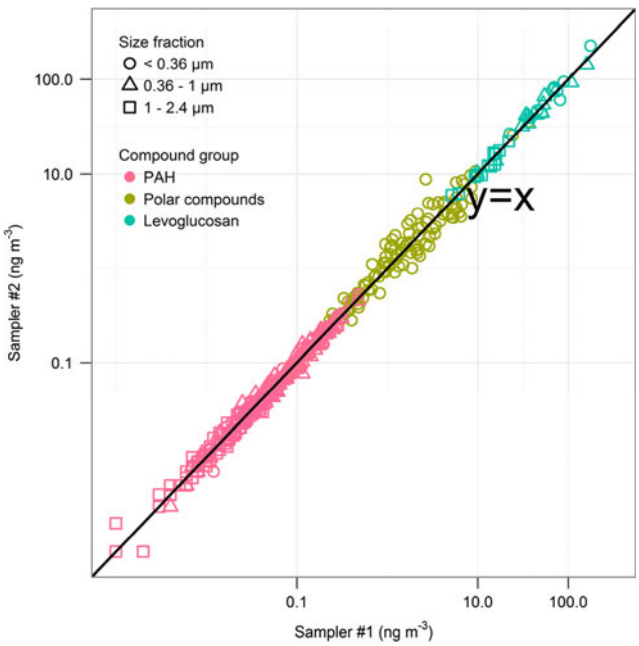

Fig. 3 Scatter plot of measured compound concentrations from sampler set #1 and sampler set #2 with 1:1 line shown on the plot as well

Chemical compounds concentration time series

PAH and levoglucosan time series and their internal correlations

Time series of PAH and levoglucosan concentrations from different size fractions are shown in Fig. 4a (see Online Resource 1 Table S5 for the concentration means and ranges). Pearson correlation analysis results (all discussed correlation heat map see Online Resource 1 Fig. S2 and S3) show that PAH and levoglucosan measured within each size range are strongly correlated with each other. There is a strong correlation between high molecular weight (HMW) PAH (>4 ring) within each size range ($0.8 < r < 1$). The correlation between low molecular weight (LMW) PAH fluoranthene and pyrene with other HMW PAH is good but not so strong ($0.7 < r < 0.9$). In addition, PAH in 0.36–1 and 1–2.5 μm PM are also strongly and positively correlated ($0.7 < r < 1$). However, the correlations between PAH in PM <0.36 μm and the other two coarser size ranges (>0.36 μm) are generally weaker (majority of *r* in 0.5–0.8). From the above, despite the common combustion forming mechanism for PAH, the finest PM PAH show somehow different variation pattern from the other fraction PAH; and the LMW PAH shows different pattern from the HMW PAH.

PAH and levoglucosan correlation with wind speed and PNC

Figure 5 shows the average size segregated PNC (a), wind speed (b), and temperature (c). Pearson correlation analysis shows that the wind speed is more negatively correlated with PAH in PM <0.36 μm ($0.6 < r < 0.8$) than with PAH in PM 0.36–1 μm ($0.2 < r < 0.4$) (see Online Resource 1 Fig. S3). This indicates that the wind speed was an important metrological factor especially for the dispersion of the PAH in lower accumulation mode PM. The *r* values of size-segregated PAH and levoglucosan with size-segregated PNC are shown in Table 1. (see also Online Resource 1 Fig. S3). To sum up, 5–50 nm PNC is slightly negatively correlated with PAH and levoglucosan in all size fractions. 0.36–1 μm PNC is well positively correlated with PAH and levoglucosan in all size fractions. 0.05–0.36 μm PNC is more positively correlated with PAH in PM <0.36 μm than with PAH in PM 0.36–1 and 1–2.4 μm. As is shown in Fig. 5a, size fraction 5–50 nm shows a distinct time series pattern. For instance, PNC of sample 5 and 11 whose sampling time-covered weekend shows two drops in size fraction 5–50 nm in contrast to the two peaks in size fraction 0.05–0.36 and 0.36–1 μm. Meanwhile, the finest PNC dominates the number concentration counts. The distinct PNC pattern of 5–50 nm PM and its negative correlation with measured PAH could be an indication that although the finest PM is smaller than 50 nm contributed considerably to the number concentration, it demonstrates insignificant

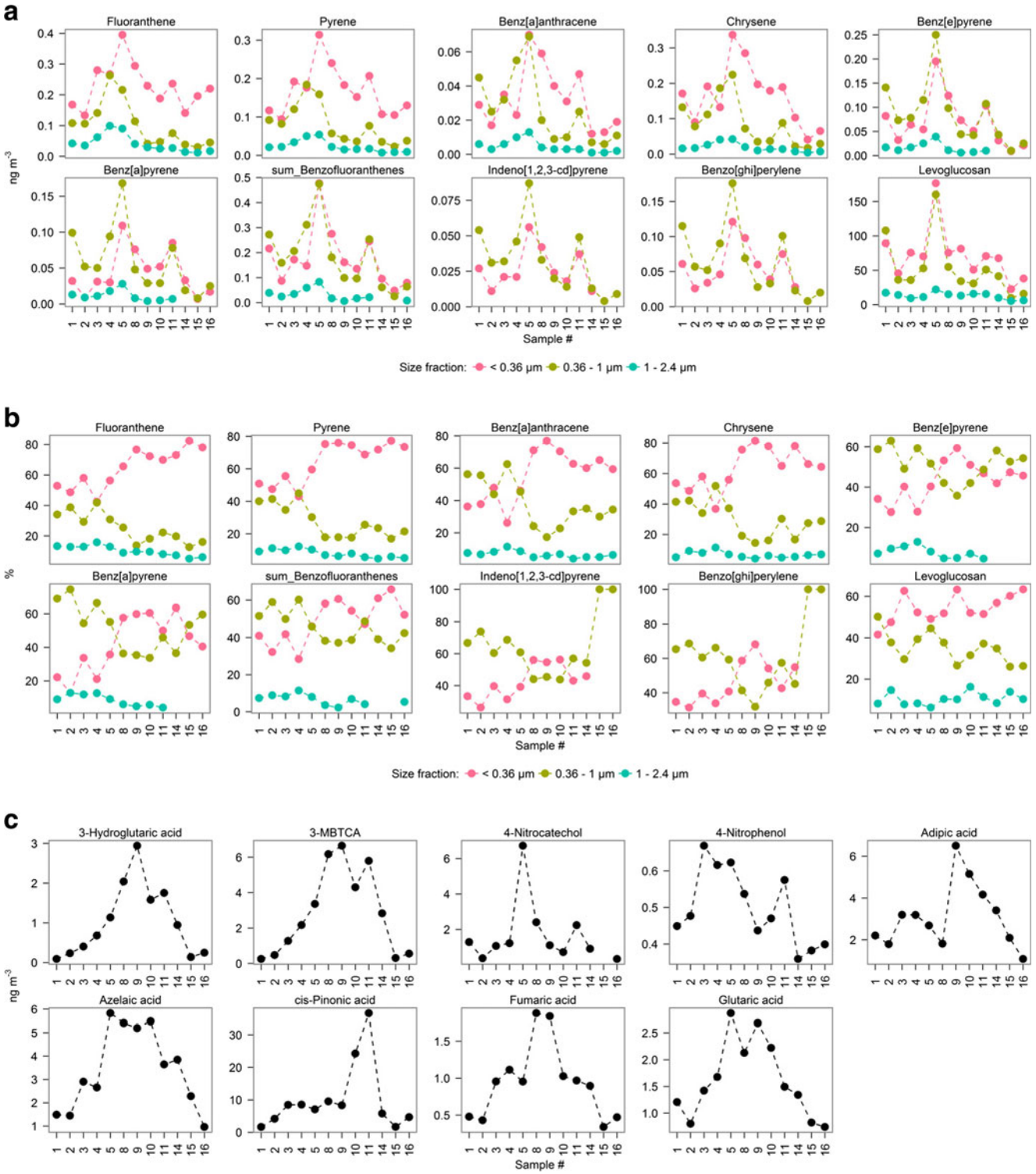

Fig. 4 Measured concentrations of PAH, levoglucosan (**a**) and polar markers (**c**) from different sample numbers (refer to Online Resource 1 Table S1 for corresponding sampling date and time, *lines between points* only intended to guide the eye); **b** calculated percentages of PAH and levoglucosan in each size range (all three size fractions add up to 100 %)

contribution to the PAH and levoglucosan during the sampling period. PM larger than 50 nm is the major contributor to PAH and levoglucosan found in these samples. Whether this is the case for other periods as well will be further investigated by our long-term sampling campaign conducted using the same sampling and measurement strategy.

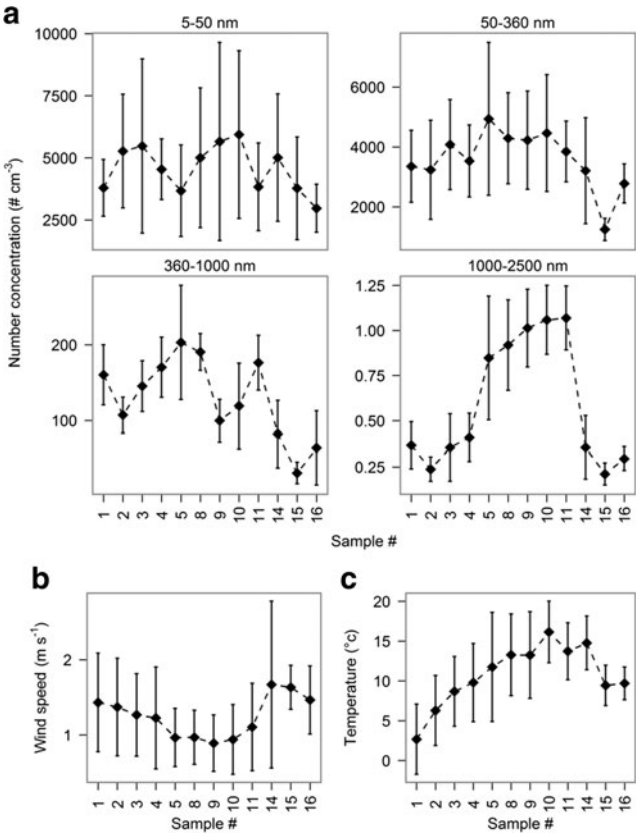

Fig. 5 **a** Measured size-segregated number concentrations (mean ± sd). **b, c** Wind speed and temperature (mean ± sd) during sampling period, respectively (*lines between points* only intended to guide the eye)

Polar marker concentrations and their correlation with wind speed, temperature, and PNC

The polar compound concentration time series is shown in Fig. 4c. These compounds provide information on the sources or oxidation status of atmospheric PM. Dicarboxylic acids are the products of photochemical reaction in the atmosphere. Very few studies have investigated these polar tracers in the fine size range (Agarwal et al. 2010; Claeys et al. 2010). Pearson correlation analysis shows that 4-nitrocatechol and 4-nitrophenol are positively correlated with PAH and levoglucosan. Whereas, the acids do not have such correlation with PAH and show distinct variation pattern as can be seen in Fig. 4. Very strong correlation ($r = 0.97$) is found between 3-hydroxyglutaric acid and 3-MBTCA, which is consistent with that they are both higher generation products of α-pinene oxidation (Szmigielski et al. 2007). Besides, except cis-pinonic acid which shows poor correlation with other acids, the rest of the acids are well positively correlated with each other ($0.5 < r < 0.9$), which might be due to the similar formation mechanism. Polar compounds in PM <0.36 μm also show high negative correlation with wind speed like PAH and levoglucosan. The correlation between acids and temperature is positive ($0.5 < r < 0.8$), and for 3-hydroxyglutaric acid, 3-MBTCA, and azelaic acid, the correlation is stronger ($r > 0.7$). This is consistent with their photochemical origin. Except for 4-nitrocatechol and 4-nitrophenol, which behave more like the PAH, other polar compounds in size fraction <0.36 μm generally have positive correlation with size-segregated PNC, especially with coarse particles >1 μm ($0.6 < r < 0.9$).

Size distribution of PAH and levoglucosan

Figure 4b shows the percentages of the PAH and levoglucosan in different size fractions. The vast majority of the PAH are found in the size range below 1 μm during this sampling period. There is less than 20 % of PAH in the PM fraction 1–2.5 μm. Spindler et al. also detected the highest PAH in the fine fraction (size ranges 0.14–0.42 μm and 0.42–1.2 μm) from 169 daily samples of 6 years of discontinuous sampling in Melpitz, Germany (Spindler et al. 2012). It can also be observed from the graph that the enrichment of the less volatile HMW PAH could be either in smallest size fraction <0.36 μm or in the size fraction of 0.36–1 μm, and the LMW PAH are more enriched in the size fraction <0.36 μm comparing to the larger molecular weight PAH. Di Filippo et al. reported a bimodal trend of LMW PAH at 0.1 and 0.4 μm and monomodal distribution of 4, 5, and 6 ring PAH at 0.4 μm of annual average in Rome, Italy (Di Filippo et al. 2010). Albinet et al. measured the size distribution of PAH (228 amu to 300 amu) in two French alpine valleys, and their result showed that in winter averagely more PAH fraction was found in the size range 0.39–1.3 μm than in the size range 0.01–0.39 μm at the near traffic site and the rural site, and vice versa at two suburban sites; in summer at all four sites more PAH fraction was found in the 0.39–1.3 μm size range (Albinet et al. 2008). Moreover, during our measurement period, a trend of elevated PAH percentages in the size fraction <0.36 μm is observed after the fourth sample. Within this time

Table 1 Pearson correlation analysis *r* range of PAH and levoglucosan in each size fraction with PNC in each size fraction

Organic size range (μm)	PNC size range (μm)			
	0.005–0.05	0.05–0.36	0.36–1	1–2.5
<0.36	−0.59–0.15	0.54–0.86	0.63–0.85	0.38–0.80
0.36–1	−0.33–0.09	0.40–0.58	0.70–0.86	−0.06–0.27
1–2.4	−0.64–0.09	0.25–0.76	0.65–0.76	−0.25–0.60

period, this change seems to be corresponding to the temperature increase shown in Fig. 5c. The factors influencing the size distributions of organic compounds could be source contribution, compound characteristics (vapor pressure, adsorption/adsorption affinity with PM, etc.), PM characteristics, and atmospheric environmental parameters (temperature, humidity, radiation and mix layer height, etc.) which influence aerosol's further chemical physical process/aging (Albinet et al. 2008; Allen et al. 1996; Venkataraman and Friedlander 1994). At this point, we could not tell whether there is a dominate factor and which it is for these increased ratios in the finest size range, or whether this is due to a comprehensive effect. This needs to be investigated further.

Summary

Collection efficiency of the last stage of the two modified 3-stage RDIs was characterized using QFFs as the substrate. The measured $C_{Dp,\ 50\%}$ is around 0.36 μm and it is much larger than the nominal value 0.1 μm. Comparing to the ungreased aluminum substrate, the measurements show that the QFF substrate altered the collection efficiency and the observed change includes decreased midpoint aerodynamic diameter and excess collection efficiency of smaller diameter PM.

A field campaign was carried out through parallel sampling using two sets of RDIs in series with filter samplers. This combination succeeded in sampling 24-h size-segregated ambient PM automatically and continuously for up to 1 week. This facilitates the investigation of the size-segregated ambient PM, especially the finest size fraction (in this case <0.36 μm). IDTD-GC-TOFMS was applied to QFF samples of all size fractions for chemical species quantification. Secondary polar markers were introduced into this method the first time, and in the finest PM fraction, they could be quantified simultaneously with PAH and levoglucosan. However, in other size fractions, only PAH and levoglucosan were quantified as the derivatization of most polar compounds was not applicable. For the purpose of field sampling in parallel at two sites required by a future epidemiological research, the comparability of these two sampling sets was verified. Firstly, the collection efficiency result shows comparable collection profile between two RDIs' last stages; secondly, the concentrations of the chemical compounds in all size fractions from two sampling sets are comparable as well.

Results from the field campaign indicate that wind speed is an important factor in influencing the chemical species in the finest PM size fraction. In addition, PM <50 nm which dominates the counts is negatively correlated with PAH in PM <0.36 μm. This indicates less contribution of the smallest PM (<50 nm) to the measured PAH. In contrast, PNCs of 50–360 and 360–1000 nm are well positively correlated to the PAH detected. In the finest size range, secondary acids show different concentration pattern from the PAH, which is consistent with their different forming mechanisms. They are found to be associated with temperature which itself is known to be related to the radiation level.

Acknowledgments This study was carried out within the framework of the project entitled "ENVIRONMENTAL NANOPARTICLES AND HEALTH: Exposure, Modeling and Epidemiology of Nanoparticles and their Composition within KORA" founded by Helmholtz Zentrum München. Additionally, Fengxia Li's PhD work is funded by the China Scholarship Council (CSC) under the State Scholarship Fund (File No. 2011601049). The authors would like to thank for this funding. We would also like to thank Dr. Yoshiteru Iinuma from the Leibniz-Institute of Troposperic Research, Leipzig, Germany, for providing the 3-MBTCA standard to enable our identification.

Compliance with ethical standards

Conflict of interest The authors declare that they have no competing interests.

References

Agarwal S, Aggarwal SG, Okuzawa K, Kawamura K (2010) Size distributions of dicarboxylic acids, ketoacids, alpha-dicarbonyls, sugars, WSOC, OC, EC and inorganic ions in atmospheric particles over Northern Japan: implication for long-range transport of Siberian biomass burning and East Asian polluted aerosols. Atmos Chem Phys 10:5839–5858

Albinet A, Leoz-Garziandia E, Budzinski H, Villenave E, Jaffrezo JL (2008) Nitrated and oxygenated derivatives of polycyclic aromatic hydrocarbons in the ambient air of two French alpine valleys—Part 2: particle size distribution. Atmos Environ 42:55–64

Allen JO, Dookeran KM, Smith KA, Sarofim AF, Taghizadeh K, Lafleur AL (1996) Measurement of polycyclic aromatic hydrocarbons associated with size-segregated atmospheric aerosols in Massachusetts. Environ Sci Technol 30:1023–1031

Bukowiecki N, Hill M, Gehrig R, Zwicky CN, Lienemann P, Hegedus F, Falkenberg G, Weingartner E, Baltensperger U (2005) Trace metals in ambient air: hourly size-segregated mass concentrations determined by Synchrotron-XRF. Environ Sci Technol 39:5754–5762

Bukowiecki N, Gehrig R, Hill M, Lienemann P, Zwicky CN, Buchmann B, Weingartner E, Baltensperger U (2007) Iron, manganese and copper emitted by cargo and passenger trains in Zurich (Switzerland): size-segregated mass concentrations in ambient air. Atmos Environ 41:878–889

Bukowiecki N, Richard A, Furger M, Weingartner E, Aguirre M, Huthwelker T, Lienemann P, Gehrig R, Baltensperger U (2009) Deposition uniformity and particle size distribution of ambient aerosol collected with a rotating drum impactor. Aerosol Sci Technol 43: 891–901

Claeys M, Graham B, Vas G, Wang W, Vermeylen R, Pashynska V, Cafmeyer J, Guyon P, Andreae MO, Artaxo P, Maenhaut W (2004) Formation of secondary organic aerosols through photooxidation of isoprene. Science 303:1173–1176

Claeys M, Kourtchev I, Pashynska V, Vas G, Vermeylen R, Wang W, Cafmeyer J, Chi X, Artaxo P, Andreae MO, Maenhaut W (2010) Polar organic marker compounds in atmospheric aerosols during the LBA-SMOCC 2002 biomass burning experiment in Rondonia,

Brazil: sources and source processes, time series, diel variations and size distributions. Atmos Chem Phys 10:9319–9331

Demokritou P, Lee SJ, Ferguson ST, Koutrakis P (2004) A compact multistage (cascade) impactor for the characterization of atmospheric' aerosols. J Aerosol Sci 35:281–299

Di Filippo P, Riccardi C, Pomata D, Buiarelli F (2010) Concentrations of PAHs, and nitro- and methyl-derivatives associated with a size-segregated urban aerosol. Atmos Environ 44:2742–2749

Gu J, Pitz M, Schnelle-Kreis J, Diemer J, Reller A, Zimmermann R, Soentgen J, Stoelzel M, Wichmann HE, Peters A, Cyrys J (2011) Source apportionment of ambient particles: comparison of positive matrix factorization analysis applied to particle size distribution and chemical composition data. Atmos Environ 45:1849–1857

Hermann M, Wiedensohler A (2001) Counting efficiency of condensation particle counters at low-pressures with illustrative data from the upper troposphere. J Aerosol Sci 32:975–991

Kavouras IG, Koutrakis P (2001) Use of polyurethane foam as the impaction substrate/collection medium in conventional inertial impactors. Aerosol Sci Technol 34:46–56

Kelly FJ, Fussell JC (2012) Size, source and chemical composition as determinants of toxicity attributable to ambient particulate matter. Atmos Environ 60:504–526

Lee SJ, Demokritou P, Koutrakis P (2005) Performance evaluation of commonly used impaction substrates under various loading conditions. J Aerosol Sci 36:881–895

Lundgren DA (1967) An aerosol sampler for determination of particle concentration as a function of size and time. J Air Pollut Control Assoc 17:225–229

Marple VA (2004) History of impactors—the first 110 years. Aerosol Sci Technol 38:247–292

Marple VA, Willeke K (1976) Impactor design. Atmopheric Environ 10: 891–896

Orasche J, Schnelle-Kreis J, Abbaszade G, Zimmermann R (2011) Technical note: in-situ derivatization thermal desorption GC-TOFMS for direct analysis of particle-bound non-polar and polar organic species. Atmos Chem Phys 11:8977–8993

Park SS, Kim YJ, Kang CH (2007) Polycyclic aromatic hydrocarbons in bulk PM2.5 and size-segregated aerosol particle samples measured in an urban environment. Environ Monit Assess 128:231–240

Pitz M, Cyrys J, Karg E, Wiedensohler A, Wichmann HE, Heinrich J (2003) Variability of apparent particle density of an urban aerosol. Environ Sci Technol 37:4336–4342

Pitz M, Birmili W, Schmid O, Peters A, Wichmann HE, Cyrys J (2008a) Quality control and quality assurance for particle size distribution measurements at an urban monitoring station in Augsburg, Germany. J Environ Monit 10:1017–1024

Pitz M, Schmid O, Heinrich J, Birmili W, Maguhn J, Zimmermann R, Wichmann HE, Peters A, Cyrys J (2008b) Seasonal and diurnal variation of PM(2.5) apparent particle density in urban air in Augsburg, Germany. Environ Sci Technol 42:5087–5093

Rao AK, Whitby KT (1978) Non-ideal collection characteristics of inertial impactors—II. Cascade impactors. J Aerosol Sci 9:87–100

Richard A, Bukowiecki N, Lienemann P, Furger M, Fierz M, Minguillon MC, Weideli B, Figi R, Flechsig U, Appel K, Prevot ASH, Baltensperger U (2010) Quantitative sampling and analysis of trace elements in atmospheric aerosols: impactor characterization and Synchrotron-XRF mass calibration. Atmos Meas Tech 3:1473–1485

Richard A, Gianini MFD, Mohr C, Furger M, Bukowiecki N, Minguillon MC, Lienemann P, Flechsig U, Appel K, DeCarlo PF, Heringa MF, Chirico R, Baltensperger U, Prevot ASH (2011) Source apportionment of size and time resolved trace elements and organic aerosols from an urban courtyard site in Switzerland. Atmos Chem Phys 11: 8945–8963

Rogula-Kozlowska W (2014) Traffic-generated changes in the chemical characteristics of size-segregated urban aerosols. Bull Environ Contam Toxicol 93:493–502

Saarikoski S, Frey A, MÃkelÃ T, Hillamo R (2008) Size distribution measurement of carbonaceous particulate matter using a low pressure impactor with quartz fiber substrates. Aerosol Sci Technol 42: 603–612

Saarnio K, Sillanpaa M, Hillamo R, Sandell E, Pennanen AS, Salonen RO (2008) Polycyclic aromatic hydrocarbons in size-segregated particulate matter from six urban sites in Europe. Atmos Environ 42:9087–9097

Sahu SK, Pandit GG, Puranik VD (2008) Dry deposition of polycyclic aromatic hydrocarbons associated with atmospheric particulate matters in an urban site, Mumbai, India. Aerosol Air Qual Res 8:437–446

Sanderson P, Delgado-Saborit JM, Harrison RM (2014) A review of chemical and physical characterisation of atmospheric metallic nanoparticles. Atmos Environ 94:353–365

Seifert M, Tiede R, Schnaiter M, Linke C, Mohler O, Schurath U, Strom J (2004) Operation and performance of a differential mobility particle sizer and a TSI 3010 condensation particle counter at stratospheric temperatures and pressures. J Aerosol Sci 35:981–993

Sillanpaa M, Hillamo R, Makela T, Pennanen AS, Salonen RO (2004) Field and laboratory tests of a high volume cascade impactor. J Aerosol Sci 34:485–500

Spindler G, Gnauk T, Gruener A, Iinuma Y, Mueller K, Scheinhardt S, Herrmann H (2012) Size-segregated characterization of PM10 at the EMEP site Melpitz (Germany) using a five-stage impactor: a six year study. J Atmos Chem 69:127–157

Szmigielski R, Surratt JD, Gomez-Gonzalez Y, Van der Veken P, Kourtchev I, Vermeylen R, Blockhuys F, Jaoui M, Kleindienst TE, Lewandowski M, Offenberg JH, Edney EO, Seinfeld JH, Maenhaut W, Claeys M (2007) 3-methyl-1,2,3-butanetricarboxylic acid: an atmospheric tracer for terpene secondary organic aerosol. Geophys Res Lett 34

Venkataraman C, Friedlander SK (1994) Size distributions of polycyclic aromatic hydrocarbons and elemental carbon. 2. Ambient measurements and effects of atmospheric processes. Environ Sci Technol 28: 563–572

Wang C, Pan Y-L, James D, Wetmore AE, Redding B (2014) Direct on-strip analysis of size- and time-resolved aerosol impactor samples using laser induced fluorescence spectra excited at 263 and 351 nm. Anal Chim Acta 820:119–132